Electromagnetic Loss Modeling and Demagnetization analysis for High Speed Permanent Magnet Machine

Yue Zhang[1], *Student Member, IEEE,* Seán McLoone[1], *Senior Member, IEEE,* and Wenping Cao[2], *Senior Member, IEEE*

[1]Queens University Belfast, Belfast, BT9 5AH, UK
[2]Aston University, Birmingham, B4 7ET, UK

This paper presents a research work on the electromagnetic loss modeling and demagnetization analysis for a high speed permanent magnet machine (HSPMM). The iron loss is estimated by improved modeling considering harmonics and rotational magnetic field effects to achieve high precision; rotor eddy current loss is researched and comprehensively investigated using finite element method (FEM). The auxiliary slot and PM beveling are also proposed to reduce the rotor eddy current loss for machine at high speed operation. Temperature-dependent PM demagnetization modeling is utilized in HSPMM FEM analysis to investigate machine performance due to temperature variation, while optimized rotor structures are proposed and comparatively researched by FEM to improve the machine anti-demagnetization capability in harsh conditions. The HSPMM temperature is estimated based on the calculated loss results and machine computational fluid dynamic (CFD) modeling. Experimental measurements on the prototype machine verify the effectiveness of the machine electromagnetic and thermal modeling in the study.

***Index Terms*—Demagnetization, finite element method, high speed permanent magnet machine, magnetic field.**

I. Introduction

HIGH SPEED permanent magnet machines (HSPMMs) have attracted extensive interests in industrial applications (such as gas compressor and turbine), due to their excellent performance and small size [1]. Owing to the constraints of limited machine heat dissipation area, power losses may cause HSPMM overheating and even PM irreversible demagnetization, which are considered as critical issues in high speed PM machine. Therefore, accurate loss and temperature estimation modeling for HSPMM are desired.

HSPMM iron loss is significantly increased as high frequency magnetic field alternating in the stator core, and it accounts for considerable proportion in the machine total loss. Thus, accurate iron loss evaluating modeling is critical for HSPMM. Rotor eddy current loss, which is induced by stator slotting and harmonics in stator magneto force, may increase rotor operating temperature. Hence, solutions reducing high speed PM machine rotor eddy current loss are desired. Besides rotor heat, PM demagnetization can also be deteriorated by stator winding armature reaction effect, which should be carefully evaluated and addressed.

In this paper, Electromagnetic loss modeling for a 150 kW, 17000 rpm HSPMM is researched and studied. The iron loss is estimated by improved modeling with both harmonics and rotational magnetic field effects considered for high precision, while the effectiveness of the iron loss improved modeling is verified by experimental tests on the machine. In this paper, stator auxiliary slot notching and rotor PM beveling methods are proposed to reduce HSPMM rotor eddy current loss by FEM analysis. Temperature-dependent PM demagnetization modeling is applied in machine FEM analysis to evaluate HSPMM demagnetization behavior. Moreover, optimized novel rotor structures against PM demagnetization are also proposed. In this study, HSPMM CFD model is built and utilized to investigate machine temperature distribution. The HSPMM is prototyped with modeling effectiveness verified by experimental measurements.

Manuscript received April 1, 2015; revised May 15, 2015 and June 1, 2015; accepted July 1, 2015. Date of publication July 10, 2015; date of current version July 31, 2015. (Dates will be inserted by IEEE; "published" is the date the accepted preprint is posted on IEEE Xplore®; "current version" is the date the typeset version is posted on Xplore®). Corresponding author: F. A. Author (e-mail: f.author@nist.gov). If some authors contributed equally, write here, "F. A. Author and S. B. Author contributed equally." IEEE TRANSACTIONS ON MAGNETICS discourages courtesy authorship; please use the Acknowledgment section to thank your colleagues for routine contributions.

Color versions of one or more of the figures in this paper are available online at http://ieeexplore.ieee.org.

Digital Object Identifier (inserted by IEEE).

II. HSPMM Structure

HSPMM structure is shown in Fig.1 and its detailed parameters are listed in Table I. The steel core for stator and rotor is composed of low loss laminations (lamination type: B20AT1500), while high mechanical strength carbon fiber sleeve (thickness is 5 mm) is utilized for the PMs against large centrifugal force during high speed operation. The machine is arranged with axial forced air cooling through ventilation area. HSPMM is also prototyped, while Fig. 2 and 3 present the stator and prototype machine, respectively.

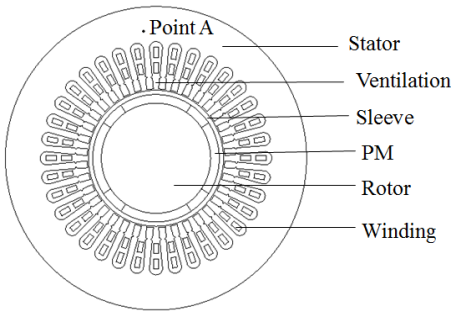

Fig. 1. HSPMM structure.

TABLE I
HSPMM PARAMETERS

Item	Val	Item	Val
Rated power (kW)	150	Rated speed (rpm)	17000
Pole pair	2	PM type	N38UH
Carbon fiber type	syt35	Stator outer diameter (mm)	350
Stator inner diameter(mm)	160	Rotor outer diameter (mm)	157
Core length (mm)	140	PM thickness (mm)	10

Fig. 2. HSPMM stator.

Fig. 3. HSPMM prototype.

III. HSPMM ELECTROMAGNETIC LOSS MODELING

A. Iron Loss modeling

Conventionally, machine iron loss is estimated by Bertotti's model with three terms: hysteresis loss P_h, eddy current loss P_c, and anomalous loss P_a, as (1):

$$p_{fe} = p_h + p_c + p_a = k_h \cdot f \cdot B_m^{\alpha} + k_c \cdot f^2 \cdot B_m^2 + k_a \cdot f^{1.5} \cdot B_m^{1.5} \quad (1)$$

where f is frequency, B_m is flux density amplitude, k_h, k_c, k_a and α are the steel hysteresis, eddy current, anomalous loss coefficients and Steinmetz coefficient. These coefficients can be obtained through Epstein test results for steel core. It is pointed out in [2] that to account for coefficient variation in high frequency, the loss coefficients k_h , k_c and α should be further modified as $k_h(f)$, $k_c(f,B_m)$ and $\alpha(f,B_m)$, which are dependent on the frequency and flux density. In this study, theses coefficients dependences are considered for HSPMM iron loss estimation.

Conventional iron loss modeling considers machine iron loss based on assumption that flux density is sinusoidal waveform only. However, the practical flux density waveform in the core is not ideal with harmonics. Fig. 4 (a) shows the radial (Br) and tangential (Bt) flux density waveforms for point A (as shown in Fig.1), while Fig. 4(b) presents the FFT analysis results for Br and Bt. It can be found that the 3th, 5th order harmonics are the main high order components in the flux density waveform which impact machine iron loss. Moreover, the core magnetization format is not only impacted by alternating magnetic field, but also rotational magnetic field, as shown in Fig 4 (c).

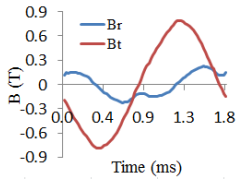

(a) Br and Bt waveforms

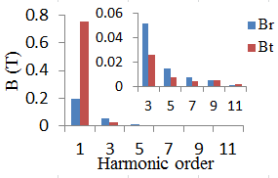

(b) FFT analysis for Br and Bt

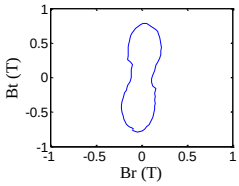

(c) Magnetization locus

Fig. 4. Flux density waveforms and magnetization locus for point A.

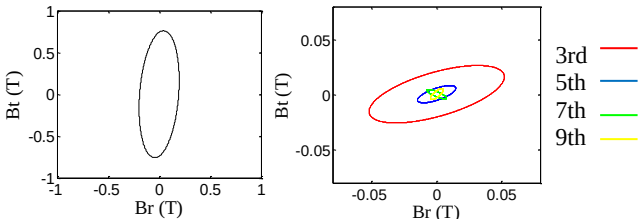

(a) fundamental (b) high order harmonics

Fig. 5. Harmonics magnetic flux loci for point A.

The additional iron loss due to rotational magnetic field is proportional to the circular degree of core magnetic flux loci. Conventional iron loss estimation method only considers the iron loss due to alternating magnetic field. The frequency of HSPMM is normally high; hence, conventional iron loss modeling is not quite applicable for machine in high speed operation due to its precision.

In order to estimate iron loss for HSPMM more accurately, it is valuable to take the core practical flux density into consideration for iron loss calculation modeling. The improved iron loss estimation modeling considering both harmonics and rotational magnetic field effects for high precision is as following: Firstly, the magnetic flux density in each region of HSPMM is obtained, and then a series of elliptical magnetic flux density loci for harmonics can be obtained by Fourier analysis. Fig. 5 shows the decomposed harmonics magnetic flux loci results for point A. The iron loss for the region can be calculated as below:

$$\begin{aligned} P_{fe} = & \sum_{k=1}^{N} k_h (kf)(kfB_{k\max}^{\alpha(kf,B_k)} + kfB_{k\min}^{\alpha(kf,B_k)}) + \\ & \sum_{k=1}^{N} k_c (kf, B_k)((kf)^2 B_{k\max}^2 + (kf)^2 B_{k\min}^2) + \\ & \frac{1}{T}\int_0^T k_a \left(\left| \frac{dB_r(t)}{dt} \right|^2 + \left| \frac{dB_t(t)}{dt} \right|^2 \right)^{\frac{3}{4}} dt \end{aligned} \quad (2)$$

where B_{kmax}, B_{kmin} are the major and minor axes of k order harmonic magnetic flux elliptical locus; B_k is k order harmonic flux density amplitude; $B_r(t)$, $B_t(t)$ are the radial and tangential components of the magnetic flux density; T is time period. Thus the total machine iron loss can be obtained by summing up the loss components in each core region.

TABLE II
HSPMM IRON LOSS AT DIFFERENT SPEEDS

Speed (rpm)		8000	11000	14000	17000
P_h(W)	Conventional	228.9	314.7	400.6	486.4
	Improved	245.2	337.1	429.1	521.3
P_c(W)	Conventional	100.7	190.4	308.5	454.8
	Improved	123.6	231.8	375.2	554.6
P_a(W)	Conventional	1.2	2.0	3.3	4.7
	Improved	1.8	2.9	4.2	5.6
P_{fe}(W)	Conventional	330.8	507.1	712.4	945.9
	Improved	370.6	571.8	808.5	1081.5
	Measured	392.8	607.5	866.3	1171.2

Table II presents the iron loss estimated by conventional modeling, improved modeling and comparison with measured values for the HSPMM at different speeds. It can be found for the machine at rated speed (17000 rpm), the extra iron loss

estimated by improved modeling is 135.6 W (accounts for around 12.5% in the total iron loss) larger than that by conventional modeling. The iron losses estimated by improved modeling are a little smaller than those measured due to factors such as temperature. Overall, the HSPMM iron losses estimation based on the improved modeling are more approaching to the measured ones at different speeds.

For the HSPMM prototype shown in Fig.3, the total loss of the machine under no load state P_{total} can be expressed as:

$$P_{total} = P_{fe} + P_{air} + P_{w} + P_{eddy} \quad (3)$$

where P_{fe}, P_{air}, P_w and P_{eddy} are the iron loss, air frictional loss, winding loss and rotor eddy current loss, respectively. Under no load condition, P_{total} is considered as machine input power which can be obtained by power analyzer in experiment. P_{air} can be estimated by CFD fluid analysis; P_w can be obtained by analytical expressions [3]; P_{eddy} is evaluated by FEM analysis. Then the machine iron loss can be obtained by loss separation. For the prototype in rated speed (17000 rpm), P_{total}, P_{air}, P_w and P_{eddy} are 4556.6W, 3252.7 W, 19.5 W and 113.2 W, respectively.

B. Rotor Eddy Current Loss

The HSPMM is assembled by surface-mounted PM with carbon fiber sleeve wrapped on PM outside. The conductivities of carbon fiber and PM are $2.2*10^4$ S/m and $6.25*10^5$ S/m, respectively. Rotor eddy current loss P_{eddy} can be estimated by time-stepping FEM analysis as:

$$P_{eddy} = \sum_{n}\left(\int \frac{|J_n|^2}{2\sigma} dv\right) \quad (4)$$

where J_n is n^{th} harmonic eddy current amplitude; σ and v are conductivity and volume. In this study, rotor eddy current loss reduction methods are proposed and analyzed with HSPMM output torque performance considered.

1. Auxiliary slot

Rectangular auxiliary slots, which notched on the stator teeth (auxiliary slots' dimensions are shown in Fig. 6), are proposed and studied to reduce HSPMM rotor eddy current loss. Fig. 7 shows the machine output torque with auxiliary slot dimensions. It can be found the machine output torque is only slightly decreased (less than 1%) before the auxiliary slot opening width (b) up to 2.5 mm. Table III presents the rotor eddy current losses in sleeve and PM with auxiliary slot dimensions when HSPMM with rated load at rated speed. For HSPMM without auxiliary slots, the eddy current losses in sleeve and PM are 120.2 W and 30.7 W, respectively. As can be found, the auxiliary slot structure with reasonable dimensions can effectively reduce machine rotor eddy current loss with little effects on machine output torque.

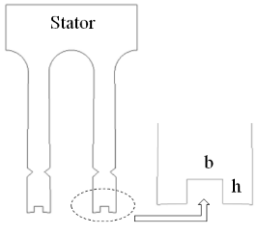

Fig. 6. Auxiliary slot.

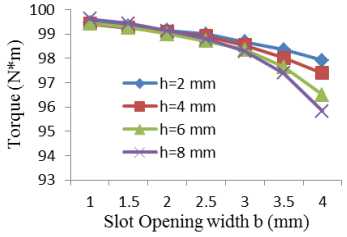

Fig. 7. Output torque with auxiliary slot dimensions

TABLE III
ROTOR EDDY CURRENT LOSS WITH AUXILIARY SLOT DIMENSIONS

	Sleeve				PM			
	b=1.0	b=1.5	b=2.0	b=2.5	b=1.0	b=1.5	b=2.0	b=2.5
h=2	120.2	110.6	98.3	90.3	30.3	28.1	25.1	23.2
h=4	117.0	105.2	96.2	87.6	29.6	26.8	24.6	22.6
h=6	116.7	104.9	91.4	78.4	29.4	26.7	23.5	20.3
h=8	116.3	103.9	87.9	74.1	29.3	26.7	22.8	19.5

2. PM beveling

PM beveling angle α is defined as shown in Fig. 8. To maintain the same output torque as the original machine, the beveled PM thickness is slightly increased to compensate the output torque loss, while the machine air gap length, rotor sleeve outer diameter and thickness are kept unchanged.

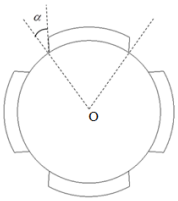

Fig. 8. PM beveling angle.

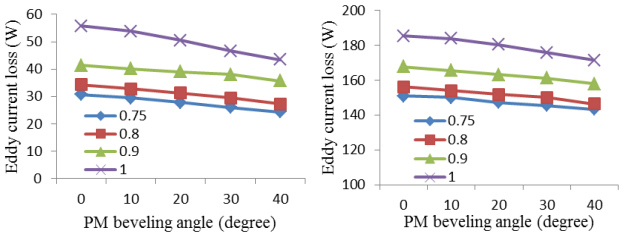

(a) PM eddy current loss (b) total rotor eddy current loss

Fig. 9. Rotor eddy current loss with PM beveling angle.

Fig. 9 presents the rotor eddy current losses for different PM pole-arc-pole-pitches (0.75, 0.8, 0.9 and 1), plotted as a function of PM beveling angles for HSPMM at rated speed with rated load. It can be found the eddy current loss can be reduced by PM beveling within the whole PM pole-arc-pole-pitch range. Take pole-arc-pole-pitch is 1.0 as example. The total rotor eddy current loss is 185.4 W without PM beveling, while it is 171.3 W for the rotor with a 40° beveling angle. Moreover, the reduction in rotor power loss is mainly contributed by PMs, as the PMs' eddy current loss reduces about 20% if increasing the beveling angle from 0° to 40°.

IV. DEMAGNETIZATION MODELING AND ANALYSIS

The PM demagnetization curve is sensitive to temperature, while the temperature-dependent PM B-H curve can be derived in [4]. Based on a set of discrete data describing PM B-H curve at reference temperature T_0, the permeability of the PM recoil line at any temperature can be modeled as:

$$\mu(T) = \left.\frac{\partial B_i(H,T)}{\partial H}\right|_{H=0} + \mu_0 = \frac{P(T)}{Q(T)}\mu_i(T_0) + \mu_0 \quad (5)$$

where

$$B_i(H,T) = P(T)\left(b_0 \tanh\left(\frac{H+Q(T)H_{ci}(T_0)}{Q(T)h_0}\right) + b_1 \tanh\left(\frac{H+Q(T)H_{ci}(T_0)}{Q(T)h_1}\right)\right) \quad (6)$$

$$P(T) = 1 + \alpha_1 (T - T_0) + \alpha_2 (T - T_0)^2 \quad (7)$$

$$Q(T) = 1 + \beta_1 (T - T_0) + \beta_2 (T - T_0)^2 \quad (8)$$

while α_1, α_2, β_1 and β_2 are the PM coefficients which can be obtained from supplier's datasheet; b_0, b_1 and h_0, h_1 are derived by nonlinear curve fitting based on the PM B-H curve at the reference temperature T_0.

The temperature-dependent PM demagnetization modeling is utilized to investigate the HSPMM output performance variation due to temperature effects. Fig. 10 presents the machine output torque with different current excitations (2, 3 and 4 times the rated current) when the PM temperature varies as: it is initial constant at 100°C, and it raises up to 180°C at 4.5 ms before returning back to 100°C at 10 ms. Obviously, the torque cannot recover to its previous value after temperature variation as the PM demagnetization occurred when the machine excited by 3 or 4 times rated current.

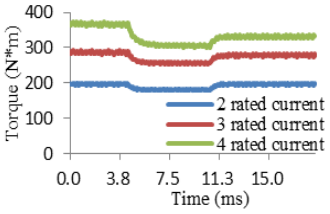

Fig. 10. HSPMM output torque with temperature variation.

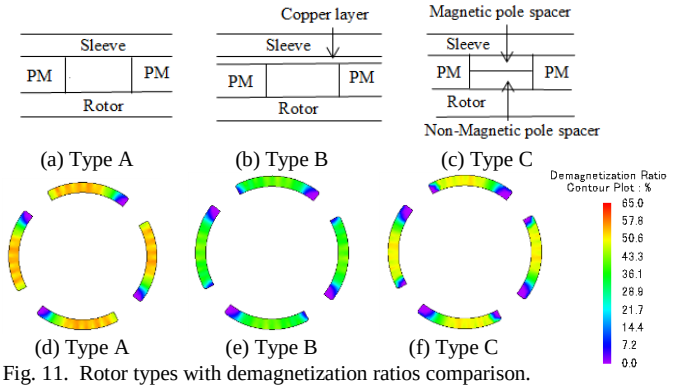

Fig. 11. Rotor types with demagnetization ratios comparison.

In this study, PM demagnetization level is assessed by demagnetization ratio, defined as the ratio of PM remanence loss after demagnetization to the original PM remanence. Fig. 11 compares the PM demagnetization with different rotor types for machine at 3-phase short circuit condition. Type A is the original rotor with surface-mounted PM, Type B is the rotor with 0.1 mm copper layer plated below the sleeve, and Type C is the rotor with two pole spacers (non-magnetic one downside and magnetic one upside). Clearly, rotor Type B and Type C can improve the machine anti-demagnetization capability in fault condition. The eddy current induced on copper layer of Type B rotor can generate a magnetic field and thus shield the PM against demagnetization. The added 0.1mm copper layer causes extra rotor eddy current loss for HSPMM at rated operation. However, copper also has higher thermal conductivity that benefiting rotor thermal dissipation. PMs' demagnetization area and level are minimized in rotor type C, as the pole spacer provides a bypass for demagnetization field, hence, alleviating the PM demagnetization risk.

V. HSPMM Thermal Model

A CFD model for one slot pitch of HSPMM is constructed to evaluate the machine temperature distribution. Power losses are regarded as heat sources, while the machine is cooled by forced air flow blowing through the ventilation region. Rotor moving is considered by setting moving wall condition on rotor surface in the model. Fig. 12 presents the CFD results for HSPMM at rated condition, while the hottest spot occurs in the middle of the rotor. Table IV presents a comparison of calculated and measured temperature results in the winding and stator of the machine. It can be found the results by machine CFD thermal model are close to the measured ones.

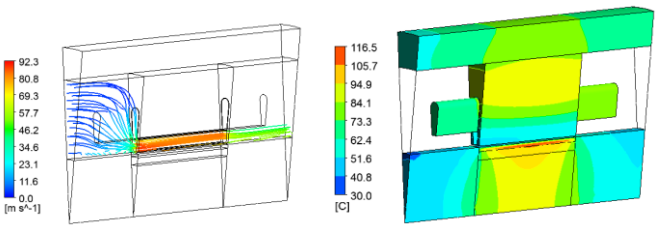

(a) Velocity streamlines (b) Temperature field distribution

Fig. 12. CFD results for HSPMM at rated speed with rated load.

TABLE IV
TEMPERATURE FOR HSPMM (°C)

	Air flow inlet		Air flow outlet	
	Winding	Stator	Winding	Stator
CFD	65.7	52.6	81.2	62.9
Measurement	66.5	51.5	82.6	64.6

VI. Conclusion

This paper introduces the electromagnetic loss modeling for a HSPMM with forced air cooling, and machine demagnetization performance is studied by temperature-dependent PM modeling. Compared with conventional modeling, improved iron loss modeling, which considers harmonics and rotational magnetic field effects, is found more accurate for HSPMM iron loss estimation. Auxiliary slots and PM beveling can effectively reduce rotor eddy current loss by FEM analysis. HSPMM demagnetization performance due to temperature variation is researched with temperature-dependent PM demagnetization modeling applied. Machine CFD model is built to estimate HSPMM temperature distribution. The effectiveness of the electromagnetic and thermal modeling is verified by experimental measurements on prototype machine.

References

[1] D. Gerada, A. Mebarki, N. Brown, and C. Gerada, "High speed electrical machines: technologies, trends, and developments," *IEEE Trans. Industrial Electronics.*, vol. 61, no. 6, pp. 2946-2959, Jun 2014.

[2] D. Ionel, M. Popescu, M. McGilp, T. Miller, S. Dellinger and R. Heideman, "Computation of core losses in electrical machines using improved models for laminated steel," *IEEE Trans. Industry Applications*, vol. 43, no. 6, pp.1554-1564, Nov/Dec. 2007.

[3] S. Jang, H. Cho and S. Choi, "Design and analysis of a high speed Brushless DC motor for centrifugal compressor," *IEEE Trans. Magnetics*, vol. 43, no. 6, pp.2573-2575, Jun. 2007.

[4] P. Zhou, D. Lin, Y. Xiao, N. Lambert and M. Rahman, "Temperature-dependent demagnetization model of permanent magnets for finite element analysis," *IEEE Trans. Magnetics*, vol. 48, no. 2, pp.1031-1034, Feb. 2012.